Redox Potentials of Chlorophylls in the Photosystem II Reaction Center†

Hiroshi Ishikita, Bernhard Loll, Jacek Biesiadka, Wolfram Saenger, and Ernst-Walter Knapp*

Institute of Chemistry, Department of Biology, Chemistry, and Pharmacy, Free University of Berlin, Takustrasse 6, D-14195 Berlin, Germany

Received September 24, 2004; Revised Manuscript Received January 6, 2005

ABSTRACT: Water oxidation generating atmospheric oxygen occurs in photosystem II (PSII), a large protein−pigment complex located in the thylakoid membrane. The recent crystal structures at 3.2 and 3.5 Å resolutions provide novel details on amino acid side chains, especially in the D1/D2 subunits. We calculated the redox potentials for one-electron oxidation of the chlorophyll *a* (Chl*a*) molecules in PSII, considering the protein environment in atomic detail. The calculated redox potentials for the dimer Chl*a* ($P_{D1/D2}$) and accessory Chl*a* ($Chl_{D1/D2}$) were 1.11−1.30 V relative to the normal hydrogen electrode at pH 7, which is high enough for water oxidation. The D1/D2 proteins and their cofactors contribute approximately 390 mV to the enormous upshift of 470 mV compared to the redox potential of monomeric Chl*a* in dimethylformamide. The other subunits are responsible for the remaining 80 mV. The high redox potentials of the two accessory Chl*a* $Chl_{D1/D2}$ suggests that they also participate in the charge separation process.

The photosynthetic reaction in photosystem II (PSII)[1] is initialized by light absorption. The resulting electronic excitation energy is ultimately converted to chemical potential starting with a charge separation process at the P680 chlorophyll *a* (Chl*a*) of the reaction center (RC), which form an oxidized positively charged radical $P680^{+\cdot}$, while the released electron travels along the electron transfer (ET) chain. The ET chain is located in the D1/D2 RC harboring two accessory Chl*a* ($Chl_{D1/D2}$), two pheophytin *a* ($Pheo_{D1/D2}$), two plastoquinones (Q_A and Q_B) from which Q_B is finally reduced. After double reduction and protonation, Q_B is released from its binding site to the bulk quinone pool associated with the thylakoidal membrane. $P680^{+\cdot}$ is re-reduced by the redox-active tyrosine D1-Tyr161, which is subsequently reduced by an electron from the Mn cluster, the heart of the oxygen-evolving complex. Ultimately, the oxidation of the Mn cluster is achieved by the high redox potential of P680 formed by Chl*a* from the RC. However, efforts to directly measure the redox potential of P680, E_m^{ox}(P680), for one-electron oxidation by spectroscopic methods were hampered by the complexity of overlapping pigment contributions in the PSII absorption spectrum near 680 nm. Therefore, the redox potential of P680 could only be deduced approximately, yielding a value of +1150 mV (*1*). A more recent estimate based on charge recombination data amounts to +1260 mV (*2*). Although these redox potentials are higher than the minimum value of +820 mV required for the oxidation of water (*3*), the enormous upshift of E_m(Chl*a*) from P680 in PSII with respect to that from monomeric Chl*a* in dimethylformamide (DMF) of +830 mV (*4*) is a matter of debate. Even less reliable is information available on the redox potentials of the other Chl*a* in PSII.

The latest crystal structure at 3.2 Å resolution (3.2-Å structure) (*5*) and the crystal structure at 3.5 Å resolution (3.5-Å structure) (*6*) of PSII isolated from the thermophilic cyanobacterium *Thermosynechococcus elongatus* revealed details of polypeptide side chains and cofactors. Here, we provide values for the redox potentials of Chl*a* molecules $P_{D1/D2}$ and $Chl_{D1/D2}$ in the PSII RC, which were calculated by solving the linearized Poisson−Boltzmann (LPB) equation accounting for all amino acids, bound redox-active cofactors, and their different charge states. The electrostatic energy computations involved titration of all charged residues and enabled us to pinpoint the direct influence of specific amino acids and cofactors on redox potential values of the cofactors in the ET chain. Because we found in our computations that the redox potentials of Chl*a* in the ET chain depend only marginally on a change of the Mn-charge state by one unit charge, i.e., $S_n \rightarrow S_{n\pm1}$ (see the Experimental Procedures), the calculated results refer to the most reduced S_0 state of PSII if not otherwise stated.

EXPERIMENTAL PROCEDURES

Coordinates. Atomic coordinates were taken from the crystal structure of PSII from *Thermosynechococcus elongatus* at resolutions of 3.2 Å (PDB 1W5C) (*5*) and 3.5 Å (PDB 1S5L) (*6*). In the former structure, a bicarbonate was added as ligand to the non-heme iron for the computation in analogy to the glutamate of the bacterial photosynthetic

† This work was supported by the Deutsche Forschungsgemeinschaft SFB 498, Projects A4 and A5, Forschergruppe Project KN 329/5-1/5-2, GRK 80/2, GRK 268, and GKR 788/1. H.I. was supported by the DAAD.

* To whom correspondence should be addressed. Telephone: (+49) 30-83854387. Fax: (+49) 30-83856921. E-mail: knapp@chemie.fu-berlin.de.

[1] Abbreviations: $Chl_{D1(D2)}$, accessory Chl*a* in D1(D2) polypeptide; bRC, bacterial photosynthetic reaction center; Chl*a*, chlorophyll *a*; $Chl_{Z(D1(D2))}$, Chl*a* of chlorophyll$_Z$ in D1(D2) polypeptide; E_m^{ox}, redox potential referring to oxidation, i.e., $Chla^0 \leftrightarrow Chla^{+\cdot}$; ET, electron transfer; LPB, linearized Poisson−Boltzmann; Mn cluster, oxygen-evolving complex with Mn ions; NHE, normal hydrogen electrode; P680, Chl*a* of PSII RC absorbing at 680 nm; $Pheo_{D1(D2)}$, pheophytin *a* in D1(D2) polypeptide; PSII, photosystem II; $P_{D1(D2)}$, dimer Chl*a* in D1(D2) polypeptide; $Q_{A(B)}$, plastoquinone in A(B) branch; RC, reaction center.

10.1021/bi047922p CCC: $30.25
Published on Web 02/12/2005

reaction center (bRC) from *Rhodobacter sphaeroides* (PDB 1AIG) (*7*). The calculated $E_m(P_{D1/D2})$ was unaffected by the presence or absence of this bicarbonate in our computation. In both crystal structures, hydrogen-atom positions were energetically optimized with CHARMM (*8*). During this procedure, the positions of all non-hydrogen atoms were fixed. All titratable groups were kept in their standard protonation states (acidic groups ionized and basic groups, including titratable histidines, protonated), and $P_{D1/D2}$, $Chl_{D1/D2}$, Chl_Z, Pheo, and plastoquinone were kept in the neutral-charge redox states. Histidines that are ligands of Chl*a* were treated as nontitratable with neutral charge.

Atomic Partial Charges. Atomic partial charges of the amino acids were adopted from the all-atom CHARMM22 (*9*) parameter set. The charges of acidic oxygens were both increased symmetrically by +0.5 unit charges to account implicitly for the presence of the proton. Similarly, instead of removing a proton in the deprotonated state, the charges of all protons of the basic groups of arginine and lysine were diminished symmetrically by a total unit charge. For residues whose protonation states are not available in the CHARMM22 parameter set, appropriate charges were computed (*10*). For the cofactors, the same atomic charges as in our previous computation of PSII (*11*) were used.

Mn Cluster. The Mn cluster is proposed to change its oxidation state from $[Mn_4]$ (II, III, and IV_2) in state S_0 to $[Mn_4]$ (III and IV_3) in states S_2 and S_3 (*12*). In the 3.5-Å structure, we considered the four explicitly given μ-oxo-oxygen atoms as O^{2-}, assigned to each Mn ion and a charge of +3.25 corresponding to the S_0 state, and included the Ca^{2+} ion and a bicarbonate that is attached to the Mn cluster, resulting in a total positive charge of +6. In the 3.2-Å structure, the Ca^{2+} ion, all four μ-oxo-bridging oxygens, and the bicarbonate are lacking in the Mn cluster. To avoid an artificial influence on calculated $P_{D1/D2}$ redox potentials because of discrepancies in atomic charges of the Mn cluster with all of its components (Ca, 4O, and bicarbonate) between the two crystal structures, the same total positive charge of six elementary units obtained for the S_0 state of the Mn_4O_4− bicarbonate complex in the 3.5-Å structure was also used for the Mn cluster in the 3.2-Å structure. Consequently, in the 3.2-Å structure, each of the four Mn ions was assigned a positive charge of +1.5 (see Table S1 in the Supporting Information).

The exact configuration of the Mn cluster is still a matter of debate. Possibly, two more oxygens than found in the 3.5-Å structure may be ligated at the Mn cluster as suggested by a recent EXAFS study (*13*). Furthermore, a Cl^- ion is also a potential ligand to the Mn cluster (*1*), although no Cl^- ion was found in the present crystal structures. Because the total charge of the Mn cluster considered to be in the S_0 state depends on the exact composition and charge state of the ligands, which so far is uncertain, we explored the influence of the charge state of the Mn cluster on the computed $E_m^{ox}(P_{D1/D2})$ by changing the total charge of the four Mn ions evenly by one unit charge to simulate $S_n \rightarrow S_{n\pm1}$ state transitions. Increasing the total charge of the Mn ions by one unit yielded an upshift of $E_m(P_{D1})$ and $E_m(P_{D2})$ by 21 and 9 mV in the 3.2-Å structure, respectively. The corresponding shifts were 25 and 12 mV in the 3.5-Å structure (*11*). Decreasing the total charge of the Mn ions by one unit downshifted $E_m(P_{D1/D2})$ by the same amount. Hence, the calculated sensitivity of $E_m(P_{D1/D2})$ to changes of the total charge of the Mn cluster is small and similar in the two crystal structures. This justifies our modeling procedure of the Mn-cluster charges regardless of differences in the explicit atomic coordinates and ligands. Thus, all computations were done in the S_0 state of the Mn cluster with the charge distribution as described above and given in detail in Table S1 of the Supporting Information.

Computation of Protonation Pattern and Redox Potentials. Our computation is based on the electrostatic continuum model by solving the LPB equation with MEAD (*14*). The protonation patterns were sampled by a Monte Carlo (MC) method with our own program Karlsberg (*15*). The dielectric constant was set to $\epsilon_P = 4$ inside the protein and $\epsilon_W = 80$ for water as done in previous computations (*11*, *16*−*20*). All computations refer to pH 7.0 at 300 K and an ionic strength of 100 mM. The LPB equation was solved using a three-step grid-focusing procedure with 2.5, 1.0, and 0.3 Å resolution. The MC sampling yields the probabilities $[A_{ox}]$ and $[A_{red}]$ of the redox states of compound A. The redox potentials are calculated from the Nernst equation

$$E = E^\circ + \frac{RT}{F}\ln\frac{[A_{ox}]}{[A_{red}]} \qquad (1)$$

where F is the Faraday constant, E is the solution redox potential. and E° is the standard redox potential of the redox-active group A. To minimize the statistical error in evaluating the redox potential, a bias potential is applied to obtain an equal amount of both redox states ($[A_{ox}] = [A_{red}]$), yielding the value of the bias potential as the resulting redox potential. For convenience, the computed redox potentials are given with millivolt accuracy, without implying that the last digit is significant. For further information about the redox potential computation and error estimate, see ref *20* and the Supporting Information. To obtain the absolute value of the redox potential in the protein, we calculated the electrostatic energy difference between the two redox states of Chl*a* in a reference model system. The shift of the redox potential in the protein relative to the reference system was added to the experimental value. As the reference model system, we used the Chl*a* redox potential versus NHE (normal hydrogen electrode) for one-electron oxidation in DMF solution $E_m^{ox}(\text{Chl}a) = +830$ mV (*4*). The DMF solution was modeled by a continuum dielectric with constant $\epsilon = 37$. The electrolyte and aprotic solvent used in electrochemical measurements affects the redox potentials. The computational method used in this study is able to consider the difference of the solvents in terms of the dielectric constant or the electrolytes in terms of ionic strength but may be limited to take all of the electrochemical factors into account. For instance, $E_m^{ox}(\text{Chl}a)$ in CH_2Cl_2 is about 60 mV lower with the electrolyte chloride−TBAC than with perchlorate−TBAP. This discrepancy was interpreted in terms of different ligation activity to $\text{Chl}a^{+\cdot}$ (*21*). Our computations ignore these effects, but all of the computational results are directly comparable, because the same reference model system, i.e., $E_m^{ox}(\text{Chl}a) = +830$ mV in DMF is used (*4*).

Dielectric Volume. The dielectric volume of a protein complex is the spatial area and shape covered by molecular

components of the protein that are the polypeptide backbone, side chains, and cofactors but not water molecules. The redox potential of a redox-active group embedded in a protein complex of low dielectric constant $\epsilon = 4$ depends on its location in the dielectric volume of the protein complex and the shape of this complex. If the redox-active group is in the center of the protein complex, it is strongly shielded from the outer solvent with $\epsilon = 80$. As a consequence, redox states where the redox-active group carries a net total charge are destabilized and protein charges near the redox-active group have a larger influence on its redox potential. In a protein with a low dielectric constant, titratable groups adopt often nonstandard protonation states (i.e., protonation/deprotonation of acidic/basic residues), which may diminish the influence of protein charges on the potential of the redox-active group. On the other hand, the influence of the protein environment diminishes considerably if a redox-active group is solvent-exposed. Hence, it adopts the redox state governed by the solution value of the redox potential. For the same reason, titratable groups that are solvent-exposed often adopt the standard protonation state, i.e., acidic groups are ionized and basic groups are protonated.

To facilitate a direct comparison with our previous computational results, we use uniformly the same computational conditions and parameters such as atomic partial charges and dielectric constants. As a general and uniform strategy, all of the crystal waters are removed in our computations (*16*−*19*, *22*−*24*) because of the lack of experimental information for hydrogen-atom positions. Cavities resulting after removal of crystal water are uniformly filled with a solvent dielectric of $\epsilon = 80$. So far, the two crystal structures of PSII do not reveal crystal waters because of the low resolution. Crystal water could have a crucial influence on E_m(Chl*a*) when it constitutes an axial ligand of Chl*a*. This might be the case for $Chl_{D1/D2}$ in PSII, because no residues are ligated to these Chl*a* in contrast to $P_{D1/D2}$ Chl*a*. The influence of crystal water on E_m(Chl*a*) generally observed in our previous computations is in the range of 20−30 mV.

Direct and Indirect Contributions to Cofactor Redox Potentials. Redox potentials of cofactors are influenced by the protein environment, which is described by the protein dielectric volume and the charge distribution generated by the amino acids. The contribution from the charges or dielectric volume of a particular residue on the shift of a cofactor redox potential can be probed by setting the residue atomic charges to zero (while keeping the van der Waals volume of the corresponding atoms at the low dielectric constant of the protein) or by deleting the atom volume from that residue, respectively. Here, we discriminate a *direct* and *indirect* contribution to the redox potential shift. The direct contribution is the bare effect of interactions between charges or the dielectric volume of the considered residue and the redox-active cofactor. The direct contribution disregards changes in the charge pattern of other titratable residues, which may occur as a consequence of the vanishing of charges or changes in the low dielectric volume of the considered residue. These changes in the charge pattern yield an additional indirect contribution to the shift in the cofactor redox potential. The direct contribution to the shift in the cofactor redox potential because of atomic charges at a specific residue is obtained if we calculate the redox potential difference between the presence and absence of charges at the particular residue, while all other charges remain invariant.

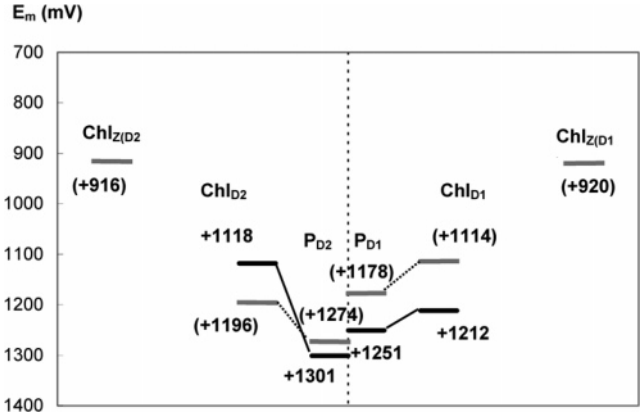

FIGURE 1: Calculated redox potentials of Chl*a* for oxidation in PSII based on the 3.2-Å structure (solid line) (*5*). The values in the bracket refer to the 3.5-Å structure (pale line) (*6*). Values are given in millivolts. Because in the 3.2-Å structure the determination of side-chain coordinates in the Chl_Z region is still incomplete, we refer to the 3.5-Å structure for the redox potentials of the cofactors $Chl_{Z(D1)}$ and $Chl_{Z(D2)}$.

RESULTS AND DISCUSSION

Remarkably High Redox Potentials of $P_{D1/D2}$ and $Chl_{D1/D2}$ for One-Electron Oxidation. The computed redox potential for oxidation is extraordinary high for the dimer Chl*a*, yielding +1251 mV for P_{D1} and +1301 mV for P_{D2} (Figure 1), as compared to the measured value of +830 mV for Chl*a* dissolved in DMF (*4*). These values are very close to +1260 mV estimated by Rappaport et al. (*2*) and large enough to oxidize Y_Z and water whose redox potentials were estimated to be between +950 and +990 mV (*25*) and +820 mV (*3*), respectively. It is notable that the same condition renders E_m^{ox} ($Chl_{Z(D1/D2)}$) be +920 and +916 mV, respectively (Figure 1), which reveals the specifically strong upshift of E_m^{ox} (Chl*a*) for $P_{D1/D2}$ and $Chl_{D1/D2}$. The lower value of +125 mV for $E_m^{ox}(P_{D1})$ compared to that of +1301 mV for $E_m^{ox}(P_{D2})$ agrees with mutation studies of the $P_{D1/D2}$ axial ligands, suggesting that $E_m^{ox}(P_{D1})$ is about 40 mV lower than $E_m^{ox}(P_{D2})$ (*26*). The computed redox potentials for the accessory Chl*a* $E_m^{ox}(Chl_{D1/D2})$ (+1212 mV for Chl_{D1} and +1118 mV for Chl_{D2}) are also nearly as large as those of $P_{D1/D2}$, which may support a multimer rather than a dimer model for the charge separation mechanism involving not only $P_{D1/D2}$ but also $Chl_{D1/D2}$ (*27*). This is corroborated by electrochemical redox titration of PSII, which showed little oxidation of Chl*a* unless very high potentials are applied (*28*).

The calculated $E_m^{ox}(Chl_{D1/D2})$ values showed an opposite redox potential pattern in the two crystal structures. Among the four Chl*a* in the RC, Chl_{D1} possesses the lowest E_m^{ox} in the 3.5-Å structure, while Chl_{D2} possesses the lowest redox potential in the 3.2-Å structure (Figure 1). One of the most straightforward interpretations of these calculated E_m^{ox} might be the following: after charge separation, the positive charge is likely to be localized at Chl_{D1} in the 3.5-Å structure and at Chl_{D2} in the 3.2-Å structure. However, according to the observation from FTIR (*29*) or absorption spectra of the $P_{D1/D2}$ axial ligand mutant (*26*), the positive charge is

delocalized on the $P_{D1/D2}$ dimer after the charge separation process. On the other hand, from a number of experimental studies, it seems likely that the primary donor for the charge separation process in PSII RC is Chl_{D1} at least at low temperatures (*30*−*35*). Prokhorenko and Holzwarth (*30*) and Dekker and van Grondelle (*31*) proposed that the electronic excitation of a multimer of Chl*a* in PSII RC proceeds initially to the $P_{D1/D2}{}^{0}Chl_{D1}{}^{+}Pheo_{D1}{}^{-}$ state. The charge-separated state in PSII RC is further stabilized by transferring the positive charge from Chl_{D1} to $P_{D1/D2}$ leading to the $P_{D1/D2}{}^{+}Chl_{D1}{}^{0}$-$Pheo_{D1}{}^{-}$ state with a time constant of ∼25 ps (*30*). At very low temperatures, the triplet state is predominantly observed at Chl_{D1} and not at $P_{D1/D2}$ (*31*). Hence, at these temperatures, there is no transfer of the positive charge from Chl_{D1} to $P_{D1/D2}$. Therefore, the transfer of the positive charge from Chl_{D1} to $P_{D1/D2}$ was proposed to be approximately isoenergetic (*31*). On the basis of the 3.5-Å structure, we computed $E_m^{ox}(Chl_{D1})$ to be 64 mV lower, while we computed $E_m^{ox}(Chl_{D2})$ to be 18 mV higher than $E_m^{ox}(P_{D1})$. Accordingly, under stationary conditions, the positive charge would be localized on Chl_{D1}. Again, this is in conflict with recent reports, which concluded that the positive charge should be at $P_{D1/D2}$ (*26*, *29*). However, we should be aware that because of the limited resolution of the PSII crystal structures underlying these computations the resulting redox potentials are subject to uncertainties.

Remarkably, in both crystal structures, Chl_{D1} has no hydrogen-bond partner. However, we found that the two crystal structures clearly differ in the orientation of the Chl_{D1} ester group whose rotation angle differs by about 180° (*5*, *6*). This difference of the Chl_{D1} ester group can change the E_m by about 60 mV, as shown in our previous computation for the accessory BChl*a* in bRC (*19*). However, it should be noted that a discrimination between the $-O-CH_3$ and $=O$ edges of the ester group in the electron-density map is very difficult at ∼3 Å or lower resolutions. Therefore, on the basis of the present PSII crystal structures (*5*, *6*), it is yet unclear which orientation of the Chl_{D1} ester group, the high- or low-potential form of Chl_{D1}, corresponding to the 3.2-Å structure or the 3.5-Å structure, respectively (see Figure 3 in ref *19*), is the relevant state for the charge separation process. The high-potential form of Chl_{D1} should energetically be more favorable for a transfer of the positive charge from Chl_{D1} to $P_{D1/D2}$ by decreasing the corresponding free-energy difference and is capable of electron-density localization in the $P_{D1/D2}{}^{+}$ state. According to mutation studies (*26*) and the present computations yielding $E_m^{ox}(P_{D1})$ lower than $E_m^{ox}(P_{D2})$, the positive charge of the $P_{D1/D2}{}^{+}$ state is localized more on P_{D1} than on P_{D2}. This promotes the ET between Y_Z and $P_{D1/D2}$ required for water oxidation at the Mn cluster. Thus, a suitable orientation of the ester group at $Chl_{D1/D2}$ might be important for the charge separation in PSII RC by affecting $E_m^{ox}(Chl_{D1/D2})$ to promote the transfer of the positive charge from Chl_{D1} to $P_{D1/D2}$, which occurs predominantly in the D1 ET branch.

Protein Charges and Dielectric Volume Influencing the $P_{D1/D2}$ Redox Potentials. One of the largest unsolved riddles of PSII is the high value of the E_m^{ox}(P680), which is needed to oxidize the redox-active D1-Tyr161 and water molecule. A large upshift of E_m^{ox}(P680) because of strong hydrogen bonds was often suggested in analogy to observations in bRC

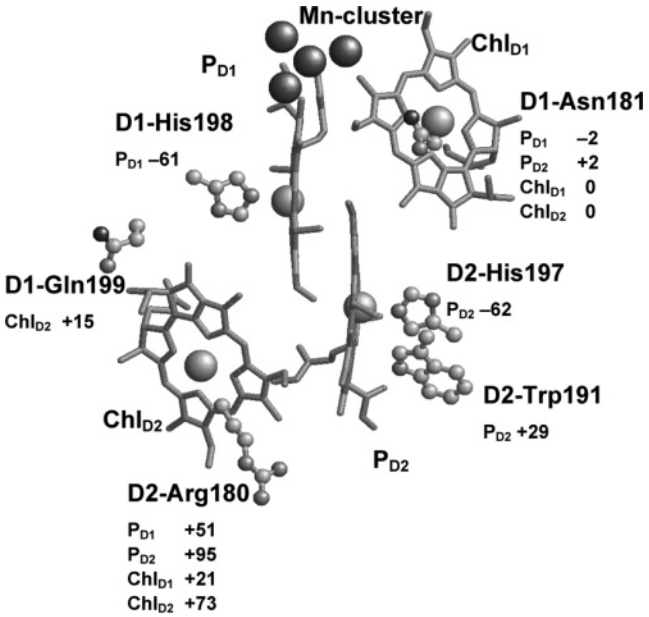

FIGURE 2: Contribution of individual residues to the redox potentials for oxidation. Positive values refer to upshifts of Chl*a* redox potentials in PSII, and negative values refer to downshifts. Values are given in millivolts. D1-Asn181 and D2-Arg180 are symmetrical counterparts in D1 and D2. D1-His198 and D2-His197 are axial ligands of Chl*a* in $P_{D1/D2}$. The figure is based on atomic corrdinates from PSII crystal structure at 3.2 Å resolution (*5*).

where the special pair redox potential may increase from +500 mV in wild-type bRC to more than +800 mV in specific mutants with hydrogen-bonding numbers enhanced by up to four bonds (*36*, *37*). This, however, is not the case for PSII, because the crystal structure clearly shows that P_{D1}, P_{D2}, and Chl_{D1} are not involved in any hydrogen bonds. Although there exists a weak hydrogen bond between Chl_{D2} and D1-Gln199, our computation yielded only a small direct influence (see the Experimental Procedures) of 15 mV upshift in $E_m^{ox}(Chl_{D2})$ from this residue (Figure 2). After removal of all protein subunits except D1 and D2, the computed $E_m^{ox}(P_{D1/D2})$ remained at very high values (+1166 mV for P_{D1} and +1219 mV for P_{D2}) (Table 1). It is remarkable that these $E_m^{ox}(P_{D1/D2})$ potentials are still positive enough to oxidize water even if PSII would consist of only D1/D2 (D1/D2 core) and that the remaining subunits surrounding this core enhance the upshift of $E_m^{ox}(P_{D1/D2})$ by 80−90 mV (Table 1). For this reason, we focus below on the D1/D2 core of PSII to clarify the factors contributing to the remaining upshift of $E_m^{ox}(P_{D1/D2})$.

Elimination of all atomic charges of polypeptide chains and cofactors in the D1/D2 core except for $P_{D1/D2}$, without varying the dielectric volume decreased $E_m^{ox}(P_{D1/D2})$ by 200−230 mV (Table 1). The remaining shift in $P_{D1/D2}$ redox potential can therefore be attributed to the dielectric volume and shape of the D1/D2 core alone, yielding 140−160 mV. This contribution is due to the exclusion of water (high dielectric) from the Chl*a* cofactors, which destabilizes the oxidized state $Chl a^{+}$ resulting in an upshift of $E_m^{ox}(P_{D1/D2})$.

The main contribution to the positive shift of $E_m^{ox}(P_{D1})$ in the D1/D2 core is associated with charges of cofactors, which yield 182 mV in total (Table 1). From this value, 129 mV is due to the Mn cluster, which according to our modeling assumptions (see the Experimental Procedures) carries a total

Table 1: Different Contributions to the $P_{D1/D2}$ Redox Potential for Oxidation in PSII[f]

model structure		3.2 Å		3.5 Å	
	$P_{D1/D2}$ of subunit	D2	D1	D2	D1
whole PSII	absolute value	+1301	+1251	+1274	+1178
all subunits except D1/D2		[82]	[85]	[95]	[66]
D1/D2-core [a]	absolute value	+1219	+1166	+1179	+1112
polypeptide charges		(132)	(15)	(61)	(−82)
backbone		(195)	(165)	(148)	(145)
side-chain [c]		(−63)	(−150)	(−87)	(−227)
cofactor charges		(100)	(182)	(104)	(186)
		[389]	[336]	[349]	[282]
Mn cluster [d]		(55)	(129)	(85)	(169)
other cofactors [e]		(45)	(53)	(19)	(17)
dielectric volume		(157)	(139)	(184)	(178)
Chl*a* [b] (DMF)	absolute value	+830	+830	+830	+830

[a] PSII consisting only of the D1/D2 subunits and the embedded cofactors ($P_{D1/D2}$, $Chl_{D1/D2}$, $Pheo_{D1/D2}$, bicarbonate, and non-heme iron). [b] See ref *4*. [c] Titrated. [d] Including a negatively charged bicarbonate. [e] Other cofactors: Chl*a*, Pheo*a*, and non-heme iron, except for Mn cluster and $P_{D1/D2}$. [f] Calculated $P_{D1/D2}$ redox potentials, accumulating the contributions from different components (dielectric volume, cofactor charges, ..., all subunits, except D1/D2) starting from the bottom with the experimental value in DMF. Redox potentials are given in millivolts. Redox potential differences (shifts) are given in brackets. Accumulated redox potentials of major components (whole PSII, D1/D2 core, and monomeric Chl*a* in DMF) are given in bold digits and connected by arrows providing the shift in rectangular brackets.

of six positive unit charges in the considered S_0 charge state. The charges of the Mn cluster also influence $E_m^{ox}(P_{D2})$, which is significantly upshifted by 55 mV, although this is only about half of the contribution computed for $E_m^{ox}(P_{D1})$. The protein backbone of the D1/D2 core significantly upshifts $E_m^{ox}(P_{D1/D2})$ by values in the range of 170−200 mV. We eliminated the atomic charges on backbone carbonyl groups and amide groups separately and calculated the resulting shift of E_m^{ox}. Accordingly, this shift can be attributed predominantly to the backbone carbonyl groups but not to the amide groups. On the other hand, charges of the amino acid side chains compensate the upshift induced by the protein backbone and even overcompensate for $E_m^{ox}(P_{D1})$ and in part for $E_m^{ox}(P_{D2})$. Thereby, the protein charges from backbones and side chains of the D1/D2 core differentiate the $E_m^{ox}(P_{D1/D2})$ redox potentials such that $E_m^{ox}(P_{D2})$ is upshifted by 117 mV relative to $E_m^{ox}(P_{D1})$. The largest individual contribution of this differentiation comes from D2-Arg180, shifting $E_m^{ox}(P_{D2})$ by +95 mV and $E_m^{ox}(P_{D1})$ by only +51 mV. On the other hand, the redox potential shift from the charge neutral residue D1-Asn181, which is the symmetry counterpart of D2-Arg180 (*38*, *39*), is vanishingly small. Thus, the subunits D1 and D2 and their bound cofactors contribute a total upshift of 336 and 389 mV, respectively, to the high value of $E_m^{ox}(P_{D1/D2})$ (see Table 1). In the calculated absolute values of $E_m^{ox}(P_{D1/D2})$ ranging between 1.25 and 1.30 V, all of these contributions to the redox potential shift are accumulated and added to the +830 mV of E_m^{ox}(Chl*a*) in DMF.

Side-Chain Charges Influencing the $P_{D1/D2}$ and $Chl_{D1/D2}$ Redox Potentials. According to our computation, the higher value of $E_m^{ox}(P_{D2})$ compared to $E_m^{ox}(P_{D1})$ was induced by the atomic charges of the protein subunits and cofactors rather than the dielectric volume and shape of the D1/D2-core part (Table 1). Here, we show the direct influence from a selection of residues in D1 and D2 on $E_m^{ox}(P_{D1/D2})$ (Figure 2). D2-Arg180, located in the neighborhood of P_{D2}, was suggested to contribute an upshift of 100−150 mV to $E_m^{ox}(P_{D1/D2})$ (*38*, *39*). This estimate correlates with our computation (51 mV for P_{D1} and 95 mV for P_{D2}), although $E_m^{ox}(P_{D2})$ is more affected than $E_m^{ox}(P_{D1})$ (Figure 2). The small edge/edge distance (∼8 Å) between the guanidinium head of D2-Arg180 and P_{D2} might be responsible for the higher value of $E_m^{ox}(P_{D2})$, while its corresponding neutral counterpart in D1, D1-Asn181, has only a marginal influence on $E_m^{ox}(P_{D1/D2})$ (Figure 2). D2-Trp191 is in van der Waals contact with P_{D2}. Many point mutations of this residue led to changes of the charge recombination kinetics, suggesting its influence on $E_m^{ox}(P_{D1/D2})$ (*40*). Although D2-Trp191 carries no net charge, we computed an upshift of $E_m^{ox}(P_{D2})$ by 29 mV because of its atomic partial charges (Figure 2).

Comparison of Protein Environment at $P_{D1/D2}$ and Chl_Z. We observed apparent differences of the contribution of the protein environment to E_m^{ox}(Chl*a*) between the pair of Chl*a* belonging to $P_{D1/D2}$ and the pair of Chl_Z. These two groups of Chl*a* are suitable examples to compare the peculiarities

of the protein environment in PSII. Both groups of Chl*a* have to be embedded in the same subunits D1/D2 and to possess one axially ligated histidine. The pure contribution of the protein dielectric volume in E_m^{ox}(Chl*a*) amounts to an upshift of only 30 mV for $E_m^{ox}(Chl_{Z(D1/D2)})$ in the 3.5-Å structure (*11*). The corresponding contribution in $E_m^{ox}(P_{D1/D2})$ resulted, however, in the much larger value of 180 mV, indicating that the low dielectric medium of the protein is upshifting E_m^{ox}(Chl*a*) roughly 6 times more for $P_{D1/D2}$ than for Chl_Z. Atomic partial charges around $P_{D1/D2}$ yield another upshift of $E_m^{ox}(P_{D1/D2})$ by 100 to 190 mV, indicating a large concentration in positive charges around $P_{D1/D2}$. The corresponding upshift of $E_m^{ox}(Chl_{Z(D1/D2)})$ was calculated to be 50−60 mV (*11*).

The $Chl_{Z(D1/D2)}$ are located at a peripheral position in contrast to $P_{D1/D2}$, with the latter being in the center of the PSII complex. Indeed, the direct influence of the atomic partial charges of the protein on $E_m^{ox}(Chl_{Z(D1/D2)})$ is comparatively small (*11*) with respect to that on $E_m^{ox}(P_{D1/D2})$, which can be related with a partial solvent exposure of Chl_Z. Thus, one might conclude that the PSII subunits surrounding the central D1/D2 chains generate an effectively lower dielectric environment around $P_{D1/D2}$ as compared to Chl_Z. However, in contrast to the large influence of the central D1/D2 chains on $E_m^{ox}(P_{D1/D2})$, the outer PSII subunits contribute only 70−100 mV to the upshift in $E_m^{ox}(P_{D1/D2})$ in our computations. Although this contribution from the outer PSII subunits is not negligible, we obtained the values of +1166/+1219 mV for $E_m^{ox}(P_{D1/D2})$ even in the absence of the outer subunits, which are still much higher than those of +920/+916 mV for $E_m^{ox}(Chl_{Z(D1/D2)})$. Thus, the highly packed protein environment around $P_{D1/D2}$ giving rise to the significant upshift of $E_m^{ox}(P_{D1/D2})$ originates predominantly from the D1/D2 chains.

CONCLUSION

In PSII, the calculated values of E_m^{ox}(P680) obtained on the basis of decoupled Chl*a* monomers were astonishingly high, namely, 1.11−1.30 V. The value of $E_m^{ox}(P_{D1})$ is lower than that of $E_m^{ox}(P_{D2})$, which is in agreement with the experiment (*26*). Our computations of E_m^{ox} (Chl*a*) in PSII revealed that the extraordinary high redox potentials for $P_{D1/D2}$ are due to the D1/D2 subunits, which contribute an upshift of about 340−390 mV, while the other subunits contribute 80−90 mV only. The main contributions from the D1/D2 subunits that upshift $E_m^{ox}(P_{D1/D2})$ and differentiate between $E_m^{ox}(P_{D1})$ and $E_m^{ox}(P_{D2})$ are (i) the polypeptide (backbone and side-chain) charges upshifting $E_m^{ox}(P_{D2})$ by 117 mV relative to $E_m^{ox}(P_{D1})$, (ii) the cofactors shifting $E_m^{ox}(P_{D1})$ and $E_m^{ox}(P_{D2})$ by 180 and 100 mV from DMF and (iii) the dielectric volume upshifting $E_m^{ox}(P_{D1})$ and $E_m^{ox}(P_{D2})$ by 140 and 160 mV from DMF, respectively.

The calculation of the E_m^{ox} (Chl*a*) in PSII demonstrates the close connections between protein complexity and redox functions of the embedded cofactors. This knowledge can serve as a basis for a deeper understanding of the PSII function and the evolution of photosynthetic proteins.

ACKNOWLEDGMENT

We thank Dr. Donald Bashford and Dr. Martin Karplus for providing MEAD and CHARMM22, respectively.

SUPPORTING INFORMATION AVAILABLE

The supporting information contains additional information on the usage of dielectric constant and atomic particle charges, more detailed error estimate, and Tables S1−S4 yielding the atomic partial charges used for the Mn cluster, bicarbonate, plastoquinone, and pheophytin in different redox states. This material is available free of charge via the Internet at http://pubs.acs.org.

REFERENCES

1. Nugent, J. H. A. (1996) Oxygenic photosynthesis, *Eur. J. Biochem. 237*, 519−531.
2. Rappaport, F., Guergova-Kuras, M., Nixon, P. J., Diner, B. A., and Lavergne, J. (2002) Kinetics and pathways of charge recombination in photosystem II, *Biochemistry 41*, 8518−8527.
3. Blankenship, R. E., and Hartman, H. (1998) The origin and evolution of oxygenic photosynthesis, *Trends Biochem. Sci. 23*, 94−97.
4. Saji, T., and Bard, A. J. (1977) Electrogenerated chemiluminescence. 29. the electrochemistry and chemiluminescence of chlorophyll *a* in *N*,*N*-dimethylformamide solutions, *J. Am. Chem. Soc. 99*, 2235−2240.
5. Biesiadka, J., Loll, B., Kern, J., Irrgang, K. D., and Zouni, A. (2004) Crystal structure of cyanobacterial photosystem II at 3.2 Å resolution: A closer look at the Mn-cluster, *Phys. Chem. Chem. Phys. 6*, 4733−4736.
6. Ferreira, K. N., Iverson, T. M., Maghlaoui, K., Barber, J., and Iwata, S. (2004) Architecture of the photosynthetic oxygen-evolving center, *Science 303*, 1831−1838.
7. Stowell, M. H. B., McPhillips, T. M., Rees, D. C., Solitis, S. M., Abresch, E., and Feher, E. (1997) Light-induced structural changes in photosynthetic reaction center: Implications for mechanism of electron−proton transfer, *Science 276*, 812−816.
8. Brooks, B. R., Bruccoleri, R. E., Olafson, B. D., States, D. J., Swaminathan, S., and Karplus, M. (1983) CHARMM: A program for macromolecular energy minimization and dynamics calculations, *J. Comput. Chem. 4*, 187−217.
9. MacKerell, A. D., Jr., Bashford, D., Bellott, R. L., Dunbrack, R. L., Jr., Evanseck, J. D., Field, M. J., Fischer, S., Gao, J., Guo, H., Ha, S., Joseph-McCarthy, D., Kuchnir, L., Kuczera, K., Lau, F. T. K., Mattos, C., Michnick, S., Ngo, T., Nguyen, D. T., Prodhom, B., Reiher, W. E., III, Roux, B., Schlenkrich, M., Smith, J. C., Stote, R., Straub, J., Watanabe, M., Wiorkiewicz-Kuczera, J., Yin, D., and Karplus, M. (1998) All-atom empirical potential for molecular modeling and dynamics studies of proteins, *J. Phys. Chem. B 102*, 3586−3616.
10. Rabenstein, B., Ullmann, G. M. and Knapp, E. W. (1998) Calculation of protonation patterns in proteins with structural relaxation and molecular ensembles−Application to the photosynthetic reaction center, *Eur. Biophys. J. 27*, 626−637.
11. Ishikita, H., and Knapp, E. W. (2005) Redox potentials of chlorophylls and β-carotene in the antenna complexes of photosystem II, *J. Am. Chem. Soc.*, in press.
12. Yachandra, V. K., Sauer, K., and Klein, M. P. (1996) Manganese cluster in photosynthesis: Where plants oxidize water to dioxygen, *Chem. Rev. 96*, 2927−2950.
13. Robblee, J. H., Messinger, J., Cinco, R. M., McFarlane, K. L., Fernandez, C., Pizarro, S. A., Sauer, K., and Yachandra, V. K. (2002) The Mn cluster in the S_0 state of the oxygen-evolving complex of photosystem II studied by EXAFS spectroscopy: Are there three di-μ-oxo-bridged Mn_2 moieties in the tetranuclear Mn complex? *J. Am. Chem. Soc. 124*, 7459−7471.
14. Bashford, D., and Karplus, M. (1990) pK_a's of ionizable groups in proteins: Atomic detail from a continuum electrostatic model, *Biochemistry 29*, 10219−10225.
15. Rabenstein, B. (1999) *Karlsberg Online Manual*, http://agknapp.chemie.fu-berlin.de/karlsberg/.
16. Ishikita, H., and Knapp, E. W. (2004) Variation of Ser-L223 hydrogen bonding with the Q_B redox state in reaction centers from *Rhodobacter sphaeroides*, *J. Am. Chem. Soc. 126*, 8059−8064.

17. Voigt, P., and Knapp, E. W. (2003) Tuning heme redox potentials in the cytochrome *c* subunit of photosynthetic reaction centers, *J. Biol. Chem. 278*, 51993−52001.
18. Ishikita, H., Morra, G., and Knapp, E. W. (2003) Redox potential of quinones in photosynthetic reaction centers from *Rhodobacter sphaeroides*: Dependence on protonation of Glu-L212 and Asp-L213, *Biochemistry 42*, 3882−3892.
19. Ishikita, H., Loll, B., Biesiadka, J., Galstyan, A., Saenger, W., and Knapp, E. W. (2005) Tuning electron transfer by ester-group of chlorophylls in bacterial photosynthetic reaction center, *FEBS Lett. 579*, 712−716.
20. Ishikita, H., and Knapp, E. W. (2003) Redox potential of quinones in both electron-transfer branches of photosystem I, *J. Biol. Chem. 278*, 52002−52011.
21. Watanabe, T., and Kobayashi, M. (1991) Electrochemistry of chlorophylls, in *Chlorophylls* (Scheer, H., Ed.) pp 287−303, CRC Press, Boca Raton, FL.
22. Rabenstein, B., Ullmann, G. M. and Knapp, E. W. (1998) Energetics of electron-transfer and protonation reactions of the quinones in the photosynthetic reaction center of *Rhodopseudomonas viridis*, *Biochemistry 37*, 2488−2495.
23. Rabenstein, B., Ullmann, G. M., and Knapp, E. W. (2000) Electron transfer between the quinones in the photosynthetic reaction center and its coupling to conformational changes, *Biochemistry 39*, 10487−10496.
24. Rabenstein, B., and Knapp, E. W. (2004) Problems evaluating energetics of electron transfer from Q_A to Q_B: The light-exposed and dark-adapted bacterial reaction center, in *Bioenergetics* (Wheeler, R. A., Ed.) pp 71−92, American Chemical Society, Washington, D.C.
25. Vass, I., and Styring, S. (1991) pH-dependent charge equilibria between tyrosine-D and the S states in photosystem II. Estimation of relative midpoint redox potentials, *Biochemistry 30*, 830−839.
26. Diner, B. A., Schlodder, E., Nixon, P. J., Coleman, W. J., Rappaport, F., Lavergne, J., Vermaas, W. F. J., and Chisholm, D. A. (2001) Site-directed mutations at D1-His198 and D2-His197 of photosystem II in *Synechocystis* PCC 6803: Sites of primary charge separation and cation and triplet stabilization, *Biochemistry 40*, 9265−9281.
27. Durrant, J. R., Klug, D. R., Kwa, S. L. S., van Grondelle, R., Porter, G., and Dekker, J. P. (1995) A multimer model for P680, the primary electron donor of photosystem II, *Proc. Natl. Acad. Sci. U.S.A. 92*, 4798−4802.
28. Rutherford, A. W., and Faller, P. (2003) Photosystem II: Evolutionary perspectives, *Philos. Trans. R. Soc. London, Ser. B 358*, 245−253.
29. Noguchi, T., Tomo, T., and Inoue, Y. (1998) Fourier transform infrared study of the cation radical of P680 in the photosystem II reaction center: Evidence for charge delocalization on the chlorophyll dimer, *Biochemistry 37*, 13614−13625.
30. Prokhorenko, V. I., and Holzwarth, A. R. (2000) Primary process and structure of the photosystem II reaction center: A photon echo study, *J. Phys. Chem. B 104*, 11563−11578.
31. Dekker, J. P., and van Grondelle, R. (2000) Primary charge separation in photosystem II, *Photosynth. Res. 63*, 195−208.
32. Barber, J., and Archer, M. D. (2001) P680, the promary electron donor of photosystem II, *J. Photochem. Photobiol., A 142*, 97−106.
33. Barber, J. (2002) P680: What is it and where is it? *Bioelectrochemistry 55*, 135−138.
34. Frese, R. N., Germano, M., de Weerd, F. L., van Stokkum, I. H. M., Shkuropatov, A. Ya., Shuvalov, V. A., van Gorkom, H. J., van Grondelle, R., and Dekker, J. P. (2003) Electric field effects on the chlorophylls, pheophytins, and β-carotenes in the reaction center of photosystem II, *Biochemistry 42*, 9205−9213.
35. Barber, J. (2004) Water, water everywhere, and its remarkable chemistry, *Biochim. Biophys. Acta 1655*, 123−132.
36. Muegge, I., Apostolakis, J., Ermler, U., Fritzsch, G., Lubitz, W., and Knapp, E. W. (1996) Shift of the special pair redox potential: Electrostatic energy computations of mutants of the reaction center from *Rhodobacter sphaeroides*, *Biochemistry 35*, 8359−8370.
37. Kalman, L., LoBrutto, R., Allen, J. P., and Williams, J. C. (1999) Modified reaction centres oxidize tyrosine in reactions that mirror photosystem II, *Nature 402*, 696−699.
38. Mulkidjanian, A. Y. (1999) Photosystem II of green plants: On the possible role of retarded protonic relaxation in water oxidation, *Biochim. Biophys. Acta 1410*, 1−6.
39. Manna, P., LoBrutto, R., Eijckelhoff, C., Dekker, J. P., and Vermaas, W. (1998) Role of Arg180 of the D2 protein in photosystem II structure and function, *Eur. J. Biochem. 251*, 142−154.
40. Keilty, A. T., Vavilin, D. V., and Vermaas, W. F. J. (2001) Functional analysis of combinatorial mutants with changes in the C-terminus of the CD loop of the D2 protein in photosystem II of *Synechocystis* sp. PCC 6803, *Biochemistry 40*, 4131−4139.

BI047922P